Chemical Engineering Journal xxx (xxxx) xxx

Contents lists available at ScienceDirect

Chemical Engineering Journal

journal homepage: www.elsevier.com/locate/cej

Field trial of hollow fiber modules of hybrid facilitated transport membranes for flue gas CO_2 capture in cement industry

Saravanan Janakiram [a], Fabio Santinelli [b], Riccardo Costi [b], Arne Lindbråthen [a], Giuseppe Marino Nardelli [b], Kris Milkowski [d], Luca Ansaloni [c], Liyuan Deng [a,*]

[a] Department of Chemical Engineering, Norwegian University of Science and Technology (NTNU), Trondheim NO-7491, Norway
[b] Colacem S.p.A., Via della Vittorina n. 60, 06024 Gubbio, PG, Italy
[c] Department of Sustainable Energy Technology, SINTEF Industry, 0373 Oslo, Norway
[d] Pilot-scale Advanced CO_2 Capture Technology (PACT) Facilities, University of Sheffield, S10 2TH Sheffield, UK

ARTICLE INFO

Keywords:
Field tests
Membrane
Facilitated transport
CO_2 capture
Flue gas
Hollow fibers

ABSTRACT

Alarming increase in global CO_2 emissions warrants acceleration of CO_2 capture technologies. In this work, testing of pre-pilot scale membrane modules containing hybrid facilitated transport membranes in hollow fiber configuration is reported. The tests were carried out using real flue gas from a slipstream in the Colacem cement plant located in Gubbio, Italy. With the fabricated modules, CO_2 flux of up to 750 NL $m^{-2}h^{-1}$ with a CO_2 permeate purity ranging from 50 to 55 vol% was recorded. All pre-pilot membrane modules showed increased CO_2 permeance in industrial testing (1.5 to 1.9x higher) compared to laboratory evaluation owing to the reliable water profile and high temperature of the flue gas from the chimney. Influence of operating parameters (e.g., pressures in the feed and permeate) were studied. Long-term testing showed no obvious reduction in permeation performance. Furthermore, the membranes with mobile carriers when exposed to the feed gas containing SO_x and NO_x exhibited good resistance to performance deterioration despite high concentrations of acidic impurities. Simulation studies based on validated experimental performance under industrial conditions reveal the high potential of the fabricated membranes as an efficient separation unit capable of achieving industrial capture rate and CO_2 purity requirements using a relatively low membrane area.

1. Introduction

Global greenhouse gas emissions have been increasing since the industrial revolution, leading to the average atmospheric CO_2 concentration rising at an alarming rate of 3 ppm(v)/year, reaching 414 ppm(v) in 2020 [1]. Overt effects of climate change in the 21st century, along with the international consensus on its direct dependence on CO_2 emissions, expedite the need for urgent implementation of emission reduction technologies. Carbon capture and storage (CCS) has been proven to be a strategic approach to significantly cut-down CO_2 emissions, especially from large-point sources like power generation, cement industries and iron and steel production facilities [2].

Although studied over decades, CCS implementation is mainly limited by the availability of versatile, environmentally benign and economically favorable technology to capture CO_2 from flue gas [3]. Among the state-of-the-art technologies for CO_2 capture, membrane technology is particularly advantageous due to its simplicity, high flexibility and modularity, low energy requirement and carbon footprint [4]. Over the past years, numerous membrane materials have been developed with improved separation properties to increase the efficiency of the flue gas treatment process [5]. Typical membrane material development involves various strategies to engineer materials that have simultaneous high CO_2 permeability and CO_2/N_2 selectivity [6]. Such membranes are usually fabricated in lab-scale as thick self-standing films. Interesting materials are then fabricated as thin-film composites (TFC) on porous supports and evaluated for separation properties using gas mixtures as feed gas [7]. In most cases, the membrane development process terminates at this juncture most likely due to the knowledge gap between lab-based research and industrial requirements or lack of a collaborative possibility to establish a constant feedback loop between technology developers and potential end-users [8]. These limitations result in only a small number of membrane materials being eventually scaled-up and tested in conditions pertinent to the targeted end-users [9]. The upscaled modules are expected to treat incoming flue gas and result in certain targets of CO_2 capture rate and CO_2 purity, depending

* Corresponding author.
E-mail address: liyuan.deng@ntnu.no (L. Deng).

https://doi.org/10.1016/j.cej.2020.127405
Received 25 July 2020; Received in revised form 20 September 2020; Accepted 15 October 2020
Available online 21 October 2020

Nomenclature

Parameters

A_{eff}	Effective membrane area [cm^{-2}]
J_{CO_2}	CO_2 flux [cm^3(STP) cm^{-2} s^{-1}]
P_F	Feed pressure [bar]
P_i	Permeance of component 'i' [GPU]
$p_{i,F}$	Partial pressure of component 'i' in the feed side [cm Hg^{-1}]
$p_{i,R}$	Partial pressure of component 'i' in the retentate side [cm Hg^{-1}]
$p_{i,P}$	Partial pressure of component 'i' in the permeate side [cm Hg^{-1}]
P_P	Permeate pressure [bar]
Vp	Total permeate flow including sweep (lab-scale tests) [ml s^{-1}]
v_P	Permeate flow rate (field tests) [cm^3(STP) s^{-1}]
x	Mole fraction of component in permeate side [Dimensionless]
y	Mole fraction of component in feed side [Dimensionless]
y_{H_2O}	Mole fraction of water in permeate [Dimensionless]
$y_{CO_2,P}$	Mole fraction of CO_2 in the permeate side [Dimensionless]
φ	Pressure ratio [Dimensionless]

Simulation variables

$\dot{V}$p	Permeate flow [Nm^3 h^{-1}]
A_{mem}	Required membrane area [m^2]
L_F	Feed flow [Nm^3 h^{-1}]
θ	Stage cut [%]

on the requirements of the end-users. Typical targets for CO_2 capture rate are over 90%, while the purity requirements of the downstream CO_2 depend on the use of the purified stream, i.e., the requirement for transport and storage is usually > 98% and varies from case to case for utilization [10,11]. In most cases, a two-stage membrane process is used to reach both targets simultaneously since the selectivity of commercially available membranes is less than 50 for CO_2/N_2 [12–14].

Recently, hybrid facilitated transport membranes (HFTMs) as hollow fibers with ultrathin selective layers (less than 200 nm) were developed, and superior separation performances were documented [15]. These HFTMs contain sterically hindered polyallylamine (SHPAA)/polyvinyl alcohol (PVA) blend as polymer matrix and size-optimized porous graphene oxide (pGO) as nanofiller at a very low loading of 0.2 wt% with respect to polymer. Additionally, CO_2-reactive small molecules were used as mobile carriers to enhance reactive transport. Lab-scale tests revealed high CO_2 permeance of up to 825 GPU for these HFTMs with a CO_2/N_2 separation factor of 31 measured at 35 °C using binary CO_2/N_2 gas mixture (10 vol% CO_2 in N_2).

In this work, three different hybrid facilitated transport membranes (HFTMs) were scaled up in hollow fiber configuration and tested with real flue gas from a cement plant. The effects of operating conditions, such as feed gas water contents and upstream and downstream pressures, on gas permeation performances were studied in detail. Long-term permeation tests lasting an extended two-week period with continuous exposure to untreated flue gas was carried out to study the durability of the fabricated pre-pilot module. The membranes consisting of mobile carriers were subject to an independent impurity testing campaign in a controlled environment to study the resistance of the membranes to SO_x and NO_x in flue gas. Consequently, the experimental results of the field tests were used as a basis to perform a stage-cut analysis of the studied membranes in a simulated single-stage membrane separation process.

2. Materials and methods

2.1. Materials

Poly(allylamine hydrochloride) (Mw = 120,000–200,000, Thermo Fisher Scientific, Sweden) was purified and converted to sterically hindered polyallylamine (SHPAA). The reaction involved the stoichiometric conversion of poly(allylamine) into poly-N-isobutyl allyl amine using potassium hydroxide (pellets, 99.9%, Sigma-Aldrich, Norway) in methanol at 50 °C under reflux conditions. [15] The precipitated SHPAA dissolved in DI water for 2 days to obtain a 6 wt% solution. Polyvinyl alcohol (Mw = 89,000–98,000, 89% hydrolyzed, Sigma-Aldrich, Norway) was dissolved in DI water at 80 °C for 4 h under reflux conditions to result in a 4 wt% solution. SHPAA and PVA were used in the ratio of 90:10 by weight.

GO used for pGO synthesis was supplied by Graphene-XT, Italy. Hydrogen peroxide (H_2O_2, 30% in water) used for pGO synthesis was supplied by Sigma Aldrich, Norway, after size optimization, as described in our previous study [15,16]. The concentration of pGO in the membrane is maintained at 0.2 wt% with respect to the total solid content in coating solution (Polymer + mobile carrier).

Mobile carriers, 1-Ethyl-3-methylimidazolium acetate ([Emim][OAc]) (97 wt%, Sigma Aldrich, Norway) was dissolved in DI water to form a 10 wt% solution. Proline-KOH (ProK) was synthesized using ι-proline (Reagentplus®, ≥99 wt%, Sigma-Aldrich, Norway) and KOH by dissolving in DI water to form a solution of 10 wt% total solids. The concentration of [Emim][OAc] content was 10%, while the polymer matrix constituted 90% by weight. Similarly, the concentration of ProK was kept at 20% (Table 1).

Poly(p-phenylene oxide) (PPO) hollow fibers (Parker A/S, Norway) with an inside diameter of 350 μm and outside diameter of 540 μm were used as support membranes.

2.2. Fabrication of pre-pilot modules

The HFTMs in this study were fabricated using a facile dip-coating method. A coating solution containing polymer, pGO nanofillers and mobile carriers (if any), with a total solid content of 0.15 wt% was used to coat individual fibers using the semi-automatic dip-coating procedure. Each fiber was coated twice in opposing directions to ensure defect-free coating of the selective layer. The thickness of the selective layer was about 200 nm. More details on the coating procedure can be found in our previous study [15]. Representative SEM images of surface and cross-section of HFTM can be found in Fig. S1 in Supplementary Information. Longer fibers were coated for pre-pilot modules when compared to lab-scale ones. Assembly into hollow fiber module was proven scalable with varying numbers of fibers, membrane area and packing density between the lab-scale and pre-pilot modules, as shown in Fig. 1. Three scaled up pre-pilot modules with membrane area ranging from

Table 1
Summary of pre-pilot module properties.

Module ID	Polymer matrix	Nanofiller	Mobile carrier	No. of fibers	Length of fibers, cm	Membrane area, cm^2
HFTM	SHPAA/PVA	0.2 wt% pGO	none	70	20	200
HFTM with 10% [Emim][OAc]	SHPAA/PVA	0.2 wt% pGO	10% [Emim] [OAc]	55	15	150
HFTM with 20% ProK	SHPAA/PVA	0.2 wt% pGO	20% ProK	55	20	175

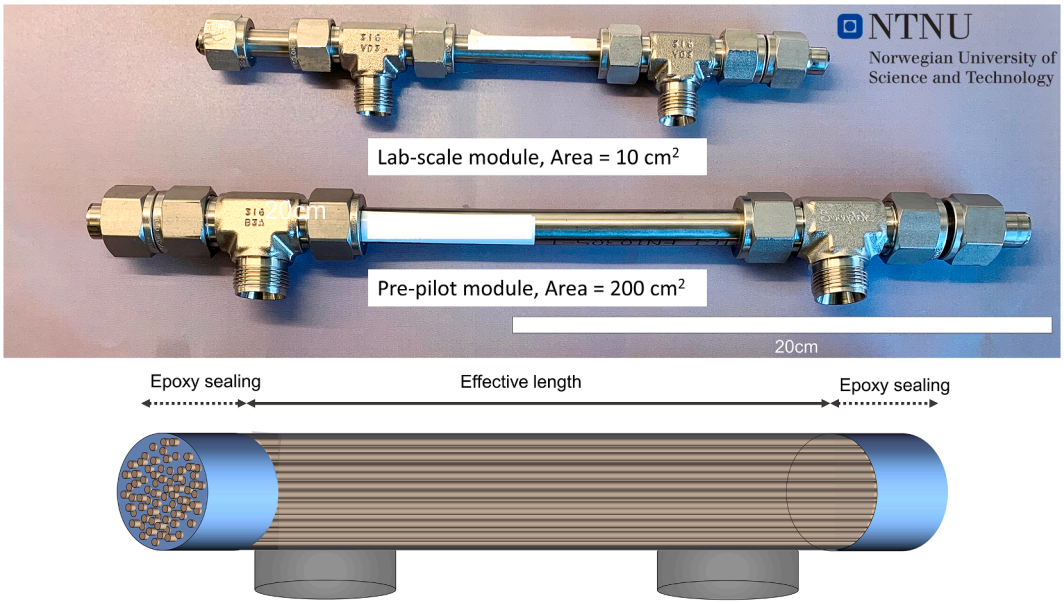

Fig. 1. Comparison of modules tested at lab-scale and pre-pilot scale.

Table 2
Combustion parameters of the kiln and flue gas properties.

Cement kiln	
Raw material feeding (t h^{-1})	~192
Fuel feeding (t h^{-1})	~9
Clinker production (t h^{-1})	~117
Stack emission components	
CO_2 (%v/v)	10.5–12.0
O_2 (%v/v)	14.0–15.5
N_2 (%v/v)	73–76
CO (ppm(v))	50–100
NO_x (ppm(v))	100–120
SO_x (ppm(v))	0–3
NH_3 (ppm(v))	20–40
HCl (ppm(v))	0.5–2

150 cm^2 to 200 cm^2 were assembled. The material configuration in the modules and the design aspects are summarised in Table 1.

2.3. In-field tests

The in-field pre-pilot testing was carried out at Colacem cement plant located in Gubbio, Italy. The production facility uses marl, limestone and small amounts of alternatives as raw materials with petroleum coke as fuel. The plant can operate at an effective clinker production capacity of 3000 tonnes day^{-1} (34.7 kg s^{-1}). The conditions of clinker production during the in-field testing and the corresponding emitted flue gas properties are furnished in Table 2.

Flue gas without major pre-treatment was used in this in-field testing campaign. The process flow diagram of the pre-pilot membrane testing system is shown in Fig. 2. The flue gas feed to the membrane module was retrieved from the emission stack from a sampling point located at a height of 75 m. A ceramic dust filter (SP180-H - M&C Tech Group, 2 μm porosity) was employed to remove particulate matter before retrieval. The flow rate of wet flue gas was at around 10–12 L min^{-1} (0.17–0.2 L s^{-1}). The membrane module was placed in a heated cabinet. The feed stream into the heated cabinet was at a temperature of 60–65 °C, while the heating cabinet was maintained at a constant temperature of 60 °C. A needle valve was used on the retentate side to control the feed pressure serving as a manual back pressure regulator. The permeate side of the membrane module was either connected to a vacuum pump or to the sweep gas depending on the tests. The compositions of permeate and retentate was measured using gas analysers - Horiba PG 350 SRM (Horiba, Japan) and Testo Model 350XL-350S (Testo, USA). The flows were measured using a flow meter, TSI 4143 (USA), and verified using a bubble flow meter. All gas lines were encased with electric heating covers with water knockouts at multiple points to prevent condensation of water and obtain desirable operating temperature.

The flue gas from the stack contained 9–11 vol% water at 115 °C. This water content corresponds to a relative humidity of 5.40 to 6.59 % RH at 1 bar and 115 °C. For the study on the water content effect on permeation properties, an additional humid stream (makeup stream) was mixed with the flue gas in an evaporator at 115 °C. The makeup stream was prepared by using a carrier gas (simulated flue gas, 12.6% CO_2/14% O_2/73.4% N_2 by volume) and DI water in a gas generator (HovaCAL® digital MF, IAS GmbH, Germany). The total water content was changed to 15 vol% and 20 vol% by using the external evaporator. The synthetic air (IP grade 20.93% O_2 and 79.07% N_2) was used in the study on the effect of feed pressures.

The gas permeation performance of the fabricated pre-pilot membrane modules was evaluated by CO_2 flux and CO_2 purity in the permeate after a single-stage operation. The CO_2 flux across the membrane was calculated by equation (1).

$$J_{CO_2} = \frac{v_P \times y_{CO_2,P}}{A_{eff}} \quad (1)$$

where J_{CO_2} is the flux in cm^3(STP) cm^{-2} s^{-1} (1 cm^3(STP) cm^{-2} s^{-1} = 10^{-2} m^3(STP) m^{-2} s^{-1} = 0.446 mol m^{-2} s^{-1}), v_P is the permeate flow rate in cm^3(STP) s^{-1} , $y_{CO_2,P}$ is the concentration of CO_2 in the permeate side and A_{eff} is the effective membrane area in cm^2. The calculated flux was verified with feed and retentate side mass balance wherever possible.

Pressure ratio (φ) is defined as the ratio of total feed pressure to total permeate pressure represented by equation (2)

$$\varphi = \frac{P_F}{P_P} \quad (2)$$

where P_F and P_P are the feed and permeate pressures in bar.

2.4. Lab-scale permeation tests

Lab-scale modules of the chosen HFTMs were also evaluated using an inhouse built humid mixed gas permeation rig at two conditions of RH. Synthetic feed gas mixture containing CO_2/N_2 mixture (10/90 v/v) was

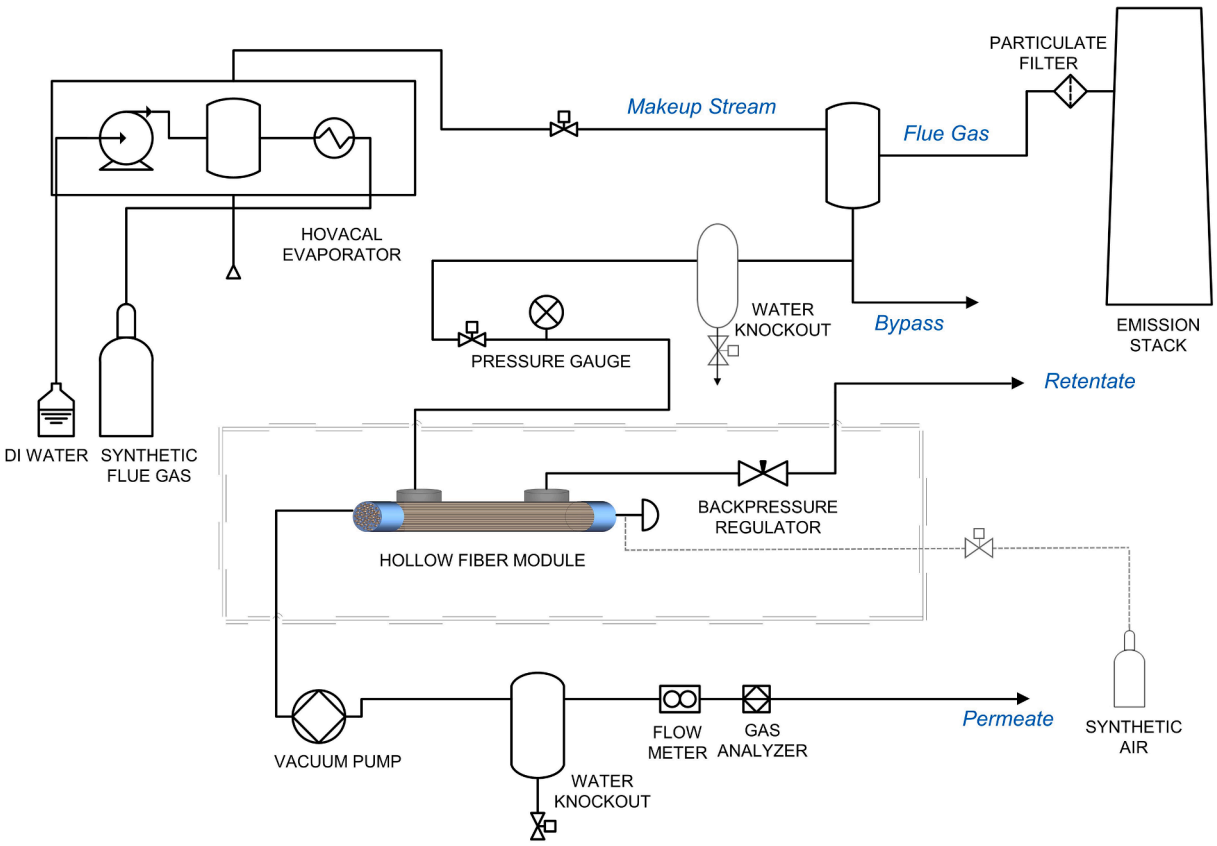

Fig. 2. Illustration of the process flow diagram of the pre-pilot membrane testing system at Colacem cement plant.

used as feed and pure CH_4 was used as the sweep gas.

The permeance of component '*i*' was obtained using the following equation

$$P_i = \frac{V_P(1 - y_{H_2O})y_i}{(\langle p_{i,F}, p_{i,R}\rangle - p_{i,P})A} \quad (3)$$

where the total permeate flow including sweep V_P (ml s^{-1}) was measured at the exit at steady state conditions using a bubble flow meter. y_{H_2O} and y_i denote the molar fraction of water and permeating species in the permeate flow, respectively. Partial pressures (in cm Hg^{-1}) are $p_{i,F}$, $p_{i,R}$ and $p_{i,P}$ of the species '*i*' in the feed, retentate and permeate, respectively. $\langle p_{i,F}, p_{i,R}\rangle$ represents the average of feed and

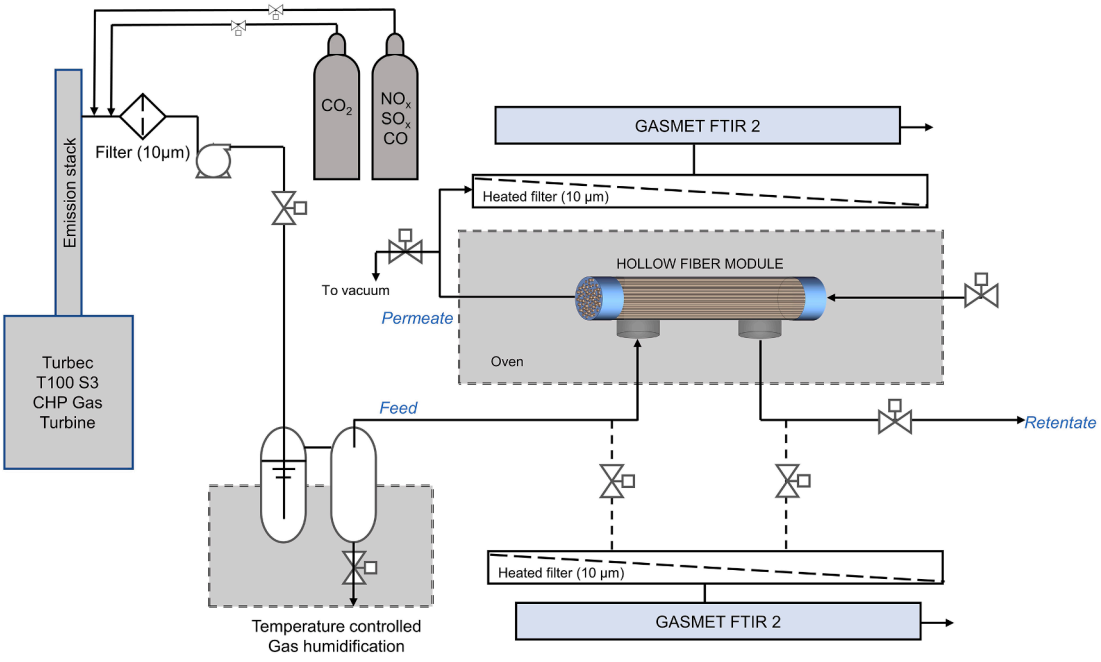

Fig. 3. Schematic of membrane testing unit at USFD.

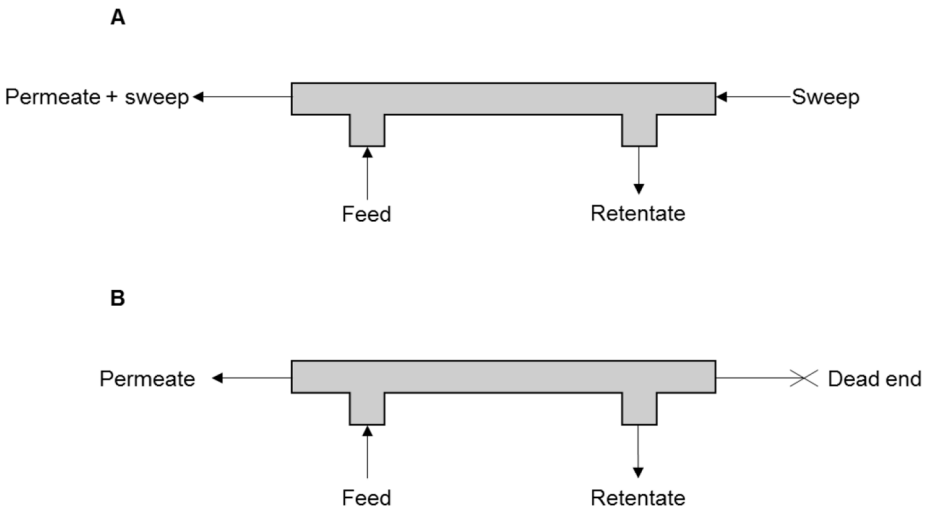

Fig. 4. Flow configuration used in modules for evaluation using (A) sweep and (B) vacuum.

retentate partial pressure determined by measuring the exit gas compositions using a pre-calibrated gas chromatograph (490 Micro GC, Agilent). Permeance of components are represented in GPU (1 GPU = 10^{-6} cm^3(STP) cm^{-2} s^{-1} $cmHg^{-1}$ = 3.35 × 10^{-10} mol m^{-2} s^{-1} Pa^{-1}). The apparent separation factor are calculated using concentrations of each component according to the equation

$$\alpha_{i/j} = \frac{y_i/x_i}{y_j/x_j} \quad (4)$$

where y and x are the gas contents in the permeate and feed side, respectively.

2.5. Accelerated aging tests

In addition to the field tests carried out at the cement industry, the HFTMs containing mobile carriers were subject to an impurity exposure testing campaign at an independent facility (Pilot-scale Advanced CO_2 Capture Technology (PACT)) at the University of Sheffield (USFD). Membranes have been integrated into a slipstream of a gas turbine with and without injection of additional CO_2 and other trace gasses to investigate performance over a range of CO_2 concentrations (1.3–30 vol %) and gas compositions representative of power generation flue gases and industrial process gases. Turbec T100 series 3 micro Combined Heat and Power (CHP) gas turbine operating on mains natural gas was utilized for the generation of flue gas for testing. Fig. 3 illustrates the overall experimental setup used for the aging tests.

Two DX4000 Gasmet FTIR (Fourier transform infrared spectroscopy) gas analysers were utilised for gas monitoring in the experimental setup, both using Calmet v11.2 data analysis software. Gasmet FTIR gas analyser 1 was connected to the monitoring of flue gas at the inlet (feed) and outlet (retentate) of the membrane (sequentially); analyser 2 was permanently connected to slipstream gas outlet for permeate analysis. Sample lines were connected via a sample conditioning unit fitted with 10-μm heated filters set at 180 °C. Analyser 1 was equipped with a 5 L min^{-1} gas sampling membrane pump. For analyser 2, the pump was disabled relaying on the sweep gas to carry the permeate gas to the sample conditioning unit and then the analyser. A 180 °C heated line interconnects the conditioning units and the FTIR analysers. The membranes were tested with nitrogen and 10% vol CO_2 feed compositions from cylinders. Initial filter and sampling pump were bypassed. Feed gas flow rates were tested from 5 to 10 L min^{-1} with the pressure of 1.7 bar (absolute). Vacuum was used in the permeate side. NO_x and SO_x were introduced from calibration gas cylinders in nitrogen at the same point and in the same manner as for CO_2.

2.6. Stage-cut analysis

For simulated membrane module performance analysis, the stage-cut and the membrane area requirement were calculated as:

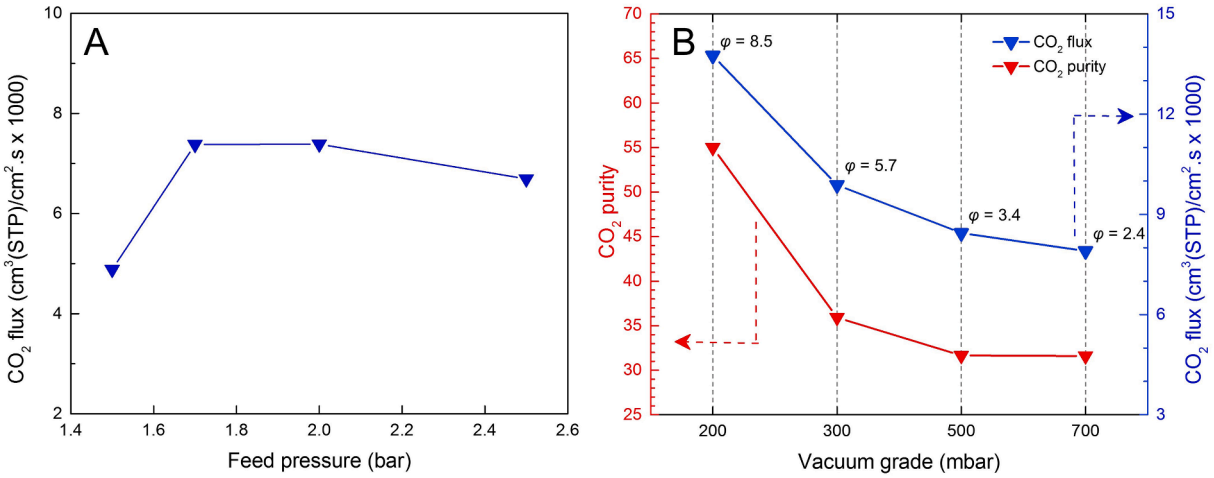

Fig. 5. Effect of (A) total pressure on feed side with sweep gas and(B) vacuum grade on permeate side (feed pressure fixed at 1.7 bar) measured at 60 °C.

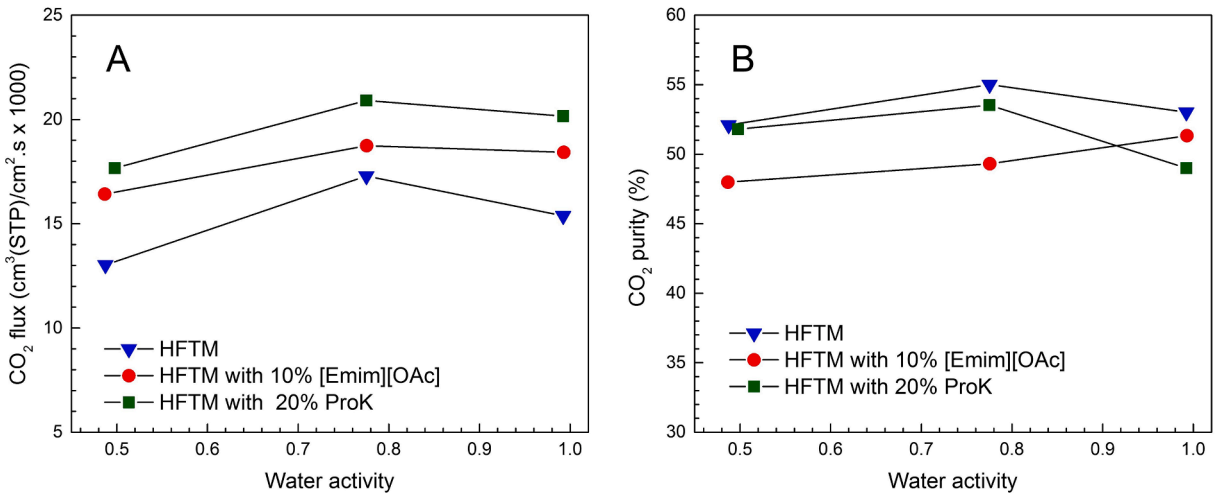

Fig. 6. Change in (A) CO_2 flux and (B) CO_2 purity of HFTMs with varying water activity in the feed measured at 60 °C, 1.7 bar feed pressure, permeate side under vacuum at 0.2 bar.

$$\theta = \frac{\dot{V}_P}{L_F} \times 100 \tag{5}$$

$$A_{req} = \frac{A_{mem}}{L_F} \tag{6}$$

where $\dot{V}_P$ is permeate and L_F is the feed volumetric flows in $Nm^3\ h^{-1}$ and A_{mem} is the membrane area required for the process in m^2.

3. Results and discussion

3.1. Effect of feed pressure and vacuum grade

The membranes considered in this study were previously evaluated for lab-scale permeation performances. The average permeance of the lab-scale modules (effective membrane area: 10–16 cm^2) was around 800 GPU, while the CO_2/N_2 separation factor was found to be around 30 for all modules measured using binary CO_2/N_2 feed gas mixture at a feed pressure of 1.7 bar and at 35 °C and fully humid conditions [15]. With the pre-pilot modules, two flow configurations were studied, as shown in Fig. 4. Configuration A uses sweep gas flowing in the bore side while feed gas flows through the shell side of the module at high pressure in a counter-current direction. This configuration reflects lab-scale evaluation under low stage-cut values, assuming complete mixing in the feed and nearly constant driving force across the module. The use of sweep gas in CO_2 separation membranes has been reported beneficial in multistage processes [17–19]. As reported by MTR, USA, in these processes, air, used as sweep gas, is concentrated with CO_2 in the second or third stage, and the CO_2-rich air is recirculated back to the combustion step [15]. The main advantage of using sweep gas in such cascades is the energy advantage for compression that is otherwise required to increase the driving force for permeation.

The use of sweep gas was studied in the HFTM module with the dry synthetic air at a constant flow rate of 3.2 LPM as the sweep gas. The CO_2 concentration in the permeate gas was ranged from 1.5 to 3 vol% and the feed pressure varied from 1.5 to 2.5 bar. Fig. 5A presents the effect of feed pressure on the CO_2 flux. As it can be seen, with increasing feed pressure from 1.5 to 1.7 bar, the CO_2 flux increased due to increasing partial pressure of CO_2 in the feed side. However, increasing the feed pressure further to up to 2.5 bar reflected no obvious changes in the flux but a trend to decrease the flux. Such behaviour is the characteristic of facilitated transport membranes due to the carrier saturation phenomenon [20]. The optimum upstream feed pressure was found to be 1.7 bar.

Given the limitations in increasing upstream feed pressure in order to create higher driving force, vacuum was used on the downstream side instead of the sweep gas to increase the transmembrane pressure difference. Unlike the use of sweep gas, using vacuum helps in concentrating CO_2 on the permeate side to high purities, making it particularly attractive for applications requiring storage or utilization of captured CO_2.

The use of vacuum (Fig. 4, configuration B) positively contributes to enhanced permeation driven by two factors: (i) increased driving force of CO_2 partial pressure between the upstream and downstream side, since the permeating gases are constantly removed by the pump and (ii) increased pressure ratio (ratio of total feed pressure to total permeate pressure, equation (2)). Pressure ratio, along with stage cut (θ) and selectivity, are the three main factors that determine the performance of a gas separation system using membranes [21]. Decreasing vacuum pressure on downstream side increases pressure ratio as seen in Fig. 5B, consequently increasing CO_2 flux across the membrane to up to 13.75×10^{-3} cm^3(STP) cm^{-2} s^{-1} at the downstream pressure of 0.2 bar which is 1.8x the maximum achievable flux using sweep at the same feed pressure. This high sensitivity of CO_2 flux to the changes in pressure ratio is because the separation happens at the so-called "pressure-ratio-limited region", where the performance of the membrane is determined solely by the pressure ratio and is independent of membrane selectivity as described by Baker [21]. While the magnitude of pressure ratio can be a theoretical maximum of infinity with the use of a high-grade vacuum, the separation eventually departs from the "pressure-ratio-limited region" and enters a "membrane-selectivity-limited region", wherein the response to pressure ratio changes are levelled off at an already achieved maximum. In the current scenario, given the lab-scale membrane selectivity is around 30, a further increase in vacuum grade could result in higher fluxes across the membrane. However, it should be noted that the pressure ratio is also an important factor that adds up to the cost of the membrane separation system and hence a very high grade of vacuum would make the process more capital and energy intensive.

3.2. Effect of water activity and temperature on performance of HFTMs

Water plays an important role in facilitated transport membranes containing reactive CO_2 carriers (Fig. S2). The water content in flue gas depends on a variety of factors such as fuel type (mainly moisture content), combustion parameters and exhaust temperature [22]. In this study, the effect of water on transport properties of the pre-pilot modules was studied by using a make-up stream of simulated flue gas carrying additional water using an external evaporator (Fig. 1). The water content in the flue gas from the chimney averaged at ~10 vol% at 115 °C

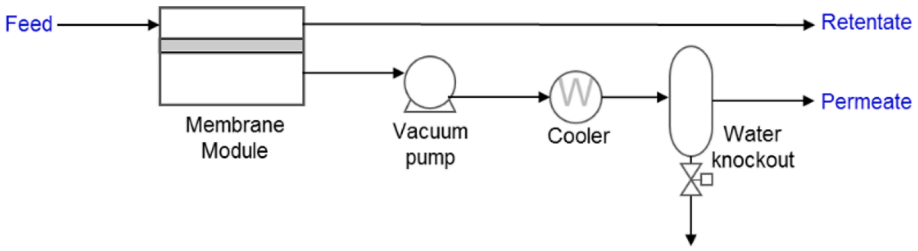

Fig. 7. Process flow diagram of single-stage membrane separation unit used for stage-cut analysis.

Table 3
Summary of separation performance of pre-pilot modules.

Module ID	Performance of pre-pilot scale membrane modules*				Performance of lab-scale membrane modules#			Maximum performance of lab-scale membrane modules±		
	Permeance (GPU)			Apparent CO_2/N_2 selectivity	Permeance (GPU)		Apparent CO_2/N_2 separation factor	Permeance (GPU)		Apparent CO_2/N_2 separation factor
	CO_2	N_2	O_2		CO_2	N_2		CO_2	N_2	
HFTM	1133.5	56.6	152.0	20.0	421.8	14.9	28.21	781.8	25.7	30.39
HFTM with 10% [Emim][OAc]	1375.8	106.8	156.1	12.9	486.9	17.95	27.12	730.6	22.6	32.27
HFTM with 20% ProK	1419.3	87.9	158.5	16.1	501.9	17.64	28.46	808.1	26.0	31.03

* measured at 60 °C/78% RH feed at 1.7 bar/vacuum 0.2 bar.
# measured at 35 °C/78% RH feed at 1.7 bar/sweep gas (also at 78% RH) at 1 bar.
± measured at 35 °C/99% RH feed at 1.7 bar/sweep gas at 1 bar.

and 1.05 bar pressure. Two more water contents corresponding to 15 vol % and 20 vol% in the feed were studied using external evaporator operating at the same temperature and pressure conditions. These water contents corresponded to ~51% RH, 78% RH and 99% RH at 1.7 bar and 60 °C.

Beyond an activity of 0.99, condensation problems occurred in the gas lines due to proximity to saturation and fluctuating temperatures at non-insulated regions of the feed gas line. All modules showed an increasing CO_2 flux and purity with increasing water activity from 0.51 to 0.78 as seen in Fig. 6. The effect of mobile carriers was eminent in the scaled-up modules in accordance with the lab scale results. At lower water activity of 0.5, both 10% [Emim][OAc] and 20% ProK containing membranes exhibited a CO_2 flux about 25% and 35% more than that of the one without any mobile carrier. This effect is attributed to the additional CO_2 transport pathway aided by the formation of carbene-adduct in the case of [Emim][OAc] [23] and carbonate/bicarbonate species in the case of ProK in the presence of water [24]. Increasing water activity to 0.78 eventually increased CO_2 flux in all modules by 15–30% than the fluxes at 0.5. A notable increase was found in HFTM without mobile carriers as the transport is mainly steered by facilitated transport mechanism via fixed-site amino groups. Higher water content leads to better utilization of amine groups in the polymer matrix, as evidenced by several studies [4,25,26]. Further increase in water content to 0.99 only resulted in marginal drops in fluxes and purities, indicating local regions of condensation in the module as the conditions are close to saturation. Nevertheless, HFTM with 10% [Emim][OAc] was an exception, where the increased water activity may have caused higher and faster association/disassociation of CO_2 with IL, thus leading to enhanced performance close to the fully humid condition.

In order to compare the performance of the pre-pilot membrane modules with the lab-scale modules, the separation performance achieved at the water activity of 0.78 (~78% RH) was chosen. In bigger modules, the concentration of CO_2 and H_2O in the feed rapidly decreases across the length of the module, and hence the driving force for permeation is no longer constant [8]. This limitation leads to the requirement of a realistic model for driving force to estimate the permeance of individual gases confidently.

To achieve the estimation of gas permeances in the pre-pilot modules, a single-stage membrane separation process mimicking the field test conditions was designed in Aspen HYSYS V9.0 integrated with an in-house built membrane model, ChemBrane. ChemBrane, with counter-current configuration, uses the 4th order Runge-Kutta method for calculating flux across the membrane module length followed by an iteration of permeance values to convergence [27]. The flow diagram described in Fig. 7 was developed in HYSYS, and the permeate and feed compositions obtained from the field tests at the water activity of 0.78 were input for simulation. Subsequently, the permeance values of gas components for each HFTM modules were calculated by manually adjusting and matching the relative ratios with ChemBrane, so that the simulated compositions of streams matched with the gas compositions measured in the exit permeate and retentate streams during the field tests for the same membrane area. The estimated permeance values for gas components in the HFTMs are summarized and compared with their respective lab-scale membrane modules in Table 3.

Sizeable differences in permeation performances from the field test conditions and the lab conditions have been observed. Two humidity levels were chosen for lab-scale investigation, i.e., 100% RH (where the potential of facilitated transport is fully utilized) and 78% RH (close to the conditions of industrial testing). The permeances of all upscaled modules at field tests were higher than that of the lab-scale ones in both cases. This phenomenon can be attributed to three important factors of difference between the different test conditions: *i)* temperature of operation, *ii)* pressure ratio, and *iii)* water profile in the feed and the module.

Given that the operating temperature in the field tests was at 60 °C as opposed to 35 °C used in lab conditions, the permeability coefficients of the membrane materials change. In usual cases, with an increase in temperature, the solubility decreases, and the diffusivity increases. Hence, the total permeability of the gas component depends on the transport mechanism of membrane material if it is solution or diffusion-dominated. Clearly, the permeances of all modules, especially the ones with mobile carriers, increased at a higher temperature. HFTM with 10% [Emim][OAc] recorded the highest increase of about 88%, followed by HFTM with 20% ProK at 76%. The HFTM without mobile carriers exhibited an increase of 45% with respect to CO_2 permeance. An increase in temperature increased the diffusivity of CO_2, more profoundly

Table 4
Viscosity and CO_2 solubility changes of mobile carriers with temperature. Data obtained from [28,29].

Temperature (°C)	ProK*		[Emim][OAc]	
	Dynamic viscosity (mPa s^{-1})	CO_2 solubility (mole fraction)	Dynamic viscosity (mPa s^{-1})	CO_2 solubility (mole fraction)
35	2.4092	0.674	74.34	0.257
60	1.400	0.594	25.19	0.189

* 2.5 M solution in water.

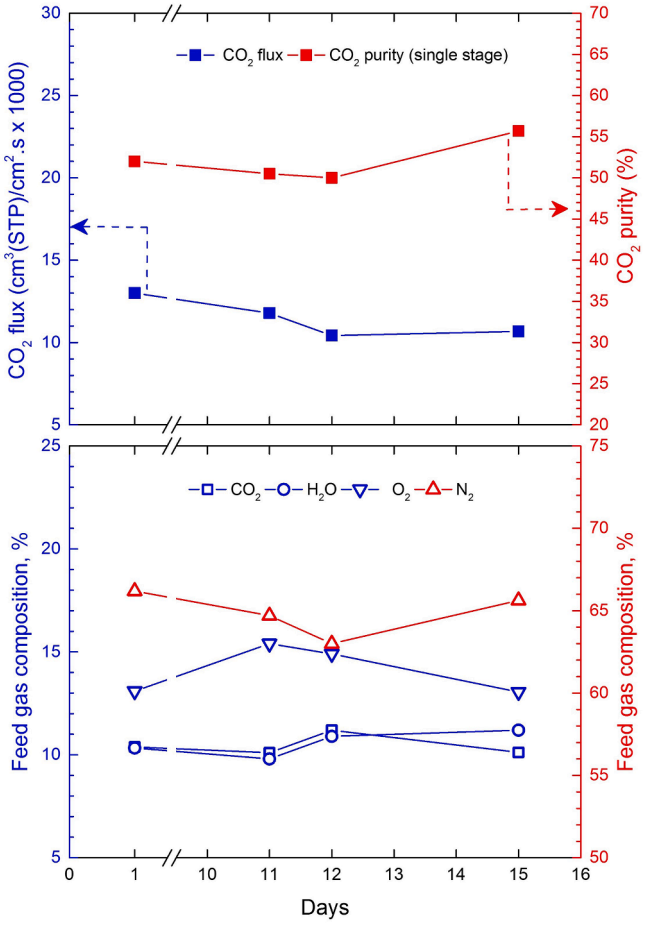

Fig. 8. Long term testing of HFTM for a period of 15 days operated at 60 °C, 1.7 bar feed pressure with permeate side under vacuum at 0.2 bar (the feed compositions are measured at 115 °C).

in membranes with mobile carriers, which confirms the potential of using mobile carriers as CO_2 reactive diffusion enhancers [15]. As expected, the apparent solubilities in these modules are reduced due to the transition towards a more diffusion-dominated mechanism as temperature increases. Evidently, membranes with [Emim][OAc] had the lowest apparent selectivity, which is in line with expectations due to the lower viscosity and reduced solubility of the IL in the membranes, as IL acts as a physical solvent at higher temperatures [28]. On the other hand, membranes with ProK suffered a smaller drop in selectivity due to relatively lower response in dynamic viscosity with respect to changing temperature, as seen in Table 4.

Another important factor for increasing CO_2 permeance is the use of vacuum on the permeate side, which leads to larger fluxes at higher pressure ratio, as described earlier. Additionally, most facilitated transport membranes document higher performance with the use of real flue gas as opposed to simulated flue gas used in laboratory evaluation; it is believed to be primarily due to the constant water content in the large volumetric flow rates from the combustion units. The additional water in the feed is also attributed to cooling down the pre-humidified flue gas from 115 °C to 60 °C [30–32], which is the operating temperature for the pilot test in this work. Compared to the lab test (at 35 °C), the faster sorption and desorption of CO_2 with amines at higher temperature can also contribute to the enhanced permeation [20,33]. Moreover, the use of pre-pilot modules of higher packing density when compared to lab scale modules results in a more reliable water profile across the length of the module, ensuring more accessible water for membrane for CO_2 facilitated transport. Besides, the larger volumetric flows lead to higher gas velocities, which results in more turbulent flow and hence reduced concentration polarization inside the modules.

3.3. Long-term stability testing of HFTM

Long-term continuous operation of membranes is necessary for evaluation of membrane performance in the pilot scale for successful separation benchmarking [34,35]. Hereof, one case (the HFTM without mobile carriers) was chosen to study the performance durability for an extended period, while the HFTMs with mobile carriers were subject to impurity testing in an independent facility. Untreated flue gas without the addition of water through external evaporator was used for this purpose. The feed pressure was maintained at 1.7 bar throughout the study. Both CO_2 flux and purity on the permeate side were recorded during the test, which lasted for about two weeks, as seen in Fig. 8. The corresponding changes in flue gas compositions were also monitored to correlate instantaneous responses to the permeation properties. It can be seen that the CO_2 flux of the module dropped slightly from 13.01 $\times$ 10^{-3} cm^3(STP) cm^{-2} s^{-1} and flattened out at $\sim$ 10.5 $\times$ 10^{-3} cm^3(STP) cm^{-2} s^{-1} after 10 days of permeation. On the other hand, the CO_2 purity remained constant at $\sim$ 51 and increasing up to $\sim$ 56 at the end of the test campaign. Clearly, the feed conditions affected the permeation properties differently. Since the facilitated transport membranes are more sensitive to the feed water content as discussed earlier, the highest water content in the feed on day 15 corresponded to the highest CO_2 purity in the module and recovery of the dropping CO_2 flux that was recorded until day 12. This point also corresponds to the lowest O_2 content in the feed gas stream. Although O_2 is considered as a contaminant in the flue gas for CO_2 separation, O_2 permeabilities are generally lower than CO_2 and higher than N_2 for all polymeric membranes [36]. While oxidative degradation is an important phenomenon in amine-based absorption systems [37], facilitated transport membranes have been reported to have shown no significant degradation with the presence of O_2 in the feed stream [31,32]. On the other hand, it should be noted that the feed flue gas was untreated except for upfront removal of particulate matter and the presence of SO_x and NO_x in trace levels did not significantly affect the membrane performance.

3.4. Effect of impurities on HFTMs with mobile carriers

Typical flue gas contains minor levels of impurities such as SO_x, NO_x, H_2S, NH_3, hydrocarbons and some heavy metals [36]. The SO_x and NO_x concentrations vary between 500 and 2000 ppm(v) and between 100 and 500 ppm(v), respectively, depending on fuel and combustion technology used [38]. The presence of SO_x and NO_x can cause irreversible changes in membranes, thereby causing a potential threat for the durability of membrane performance [39,40]. Mixtures of SO_x/NO_x and water generates sulfuric/nitric acid, which could eventually degrade the polymer chains. Conventional polymeric membrane systems typically employ flue gas desulphurisation unit and NO_x control using catalytic reduction technology prior to the membrane separation unit.

For the study of the effect of acidic contaminants in the flue gas on the membrane performance, an accelerated aging test was carried out

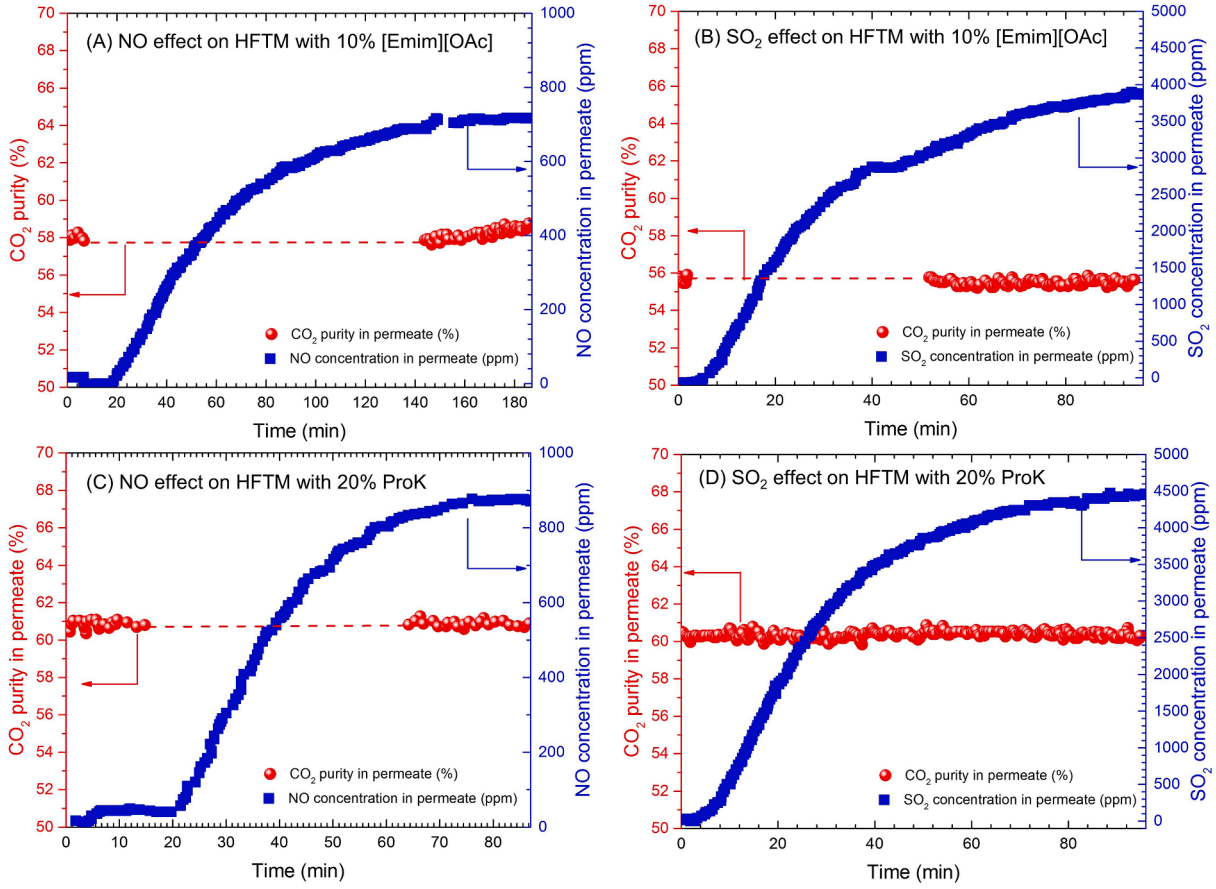

Fig. 9. Effect of SO_x and NO_x on HFTMs with mobile carriers – Effect of (A) NO and (B) SO_2 on CO_2 purity of HFTM with 10% [Emim][OAc]; Effect of (C) NO and (D) SO_2 on CO_2 purity of HFTM with 20% ProK (Average feed SO_2 composition = ~630 ppm(v); NO composition = ~380 ppm(v); membranes operated at 21 °C; 1.7 bar feed pressure; permeate side under vacuum at 0.2 bar).

with exposure of SO_2 and NO, at a composition of 630 ppm(v) and 380 ppm(v) in simulated flue gas, respectively. Only the HFTMs with mobile carriers were chosen for this test as the host polymer matrix in these membranes is similar to that of the HFTM and additionally contain small organic molecules (mobile carriers), which can be more prone to degradation. The compositions of SO_2 and NO were measured both at the feed and retentate side and the corresponding CO_2 purity in the permeate side of the membranes were monitored over time, as seen in Fig. 9. Both HFTMs containing [Emim][OAc] and ProK exhibited no changes in CO_2 purity on the permeate stream during these tests, indicating that SO_2 and NO had a negligible effect on the CO_2 transport. The effluent SO_2 and NO concentration achieved stable values in different time periods based on the composition of the membrane material. Both HFTMs concentrated SO_2 and NO on the permeate side, indicating high SO_2 and NO permeabilities in these membranes. Generally, SO_2 is expected to react with carriers and compete with CO_2 transport in facilitated transport membranes due to its high reactivity [41]. Additionally, due to their acidic nature, both SO_2 and NO change the pH of the system,

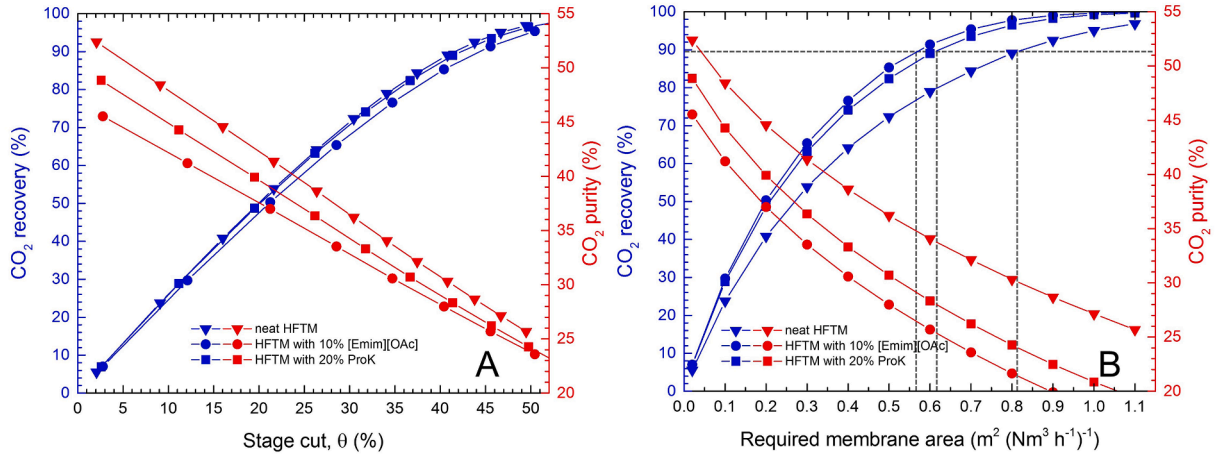

Fig. 10. Effect of stage-cut (A) and membrane area requirement (B) on CO_2 recovery and CO_2 purity (B) of HFTMs (simulated for flue gas at 60 °C; 1.7 bar feed pressure; permeate side under vacuum at 0.2 bar).

Table 5
Summary of hollow fiber membrane module performances for flue gas treatment tested at pre-pilot scale or higher.

Membrane materials	Feed Pressure	Temp (°C)	CO_2 flux (NL $m^{-2}h^{-1}$)	CO_2/N_2 selectivity/CO_2 purity (%) in permeate	Ref.
PES	6 ~ 8 bar	–	110–137*	37–47%	[48]
Prism (polysulfone)	1.32 bar	RT	~142–200	3 ~ 6	[49]
PVAm (FSC)	1 ~ 6 bar	23–45	40.1–41.4	54–56%	[32]
PVAm (FSC)	3.3 bar	39	300	83%	[31]
FTM	2 bar	RT	90.6	~40%	[9]
HFTM	1.7 bar	60	335.6–418.9	52–55%	
HFTM with 20% ProK	1.7 bar	60	529.0–603.8	47–51%	This work
HFTM with 10% [Emim][OAc]	1.7 bar	60	635.9–752.6	49–53%	

* L min^{-1}.

which in turn regulates permeation performance [42]. However, the results from the current study confirm the trend of facilitated transport membranes that documented stable performances after exposure to both SO_x and NO_x [31,43]. Nevertheless, it should be noted that the reactivity of both acidic gases with amines in the presence of water is highly dependent on temperature [44]. In the current study, the temperature of operation was maintained to 21 °C due to practical limitations, although the long-term studies document similar stability to SO_x and NO_x (Fig. 8), albeit at lower concentrations but extended operation time.

3.5. Stage-cut analysis

The separation capabilities of developed HFTMs when used in a single-stage membrane process were studied using a process simulation analysis with Aspen HYSYS V9.0. The similar flow diagram, as described in Fig. 5, was used for this purpose. The validated permeance and selectivity obtained through experimental data (Table 3) served as the basis for these simulations.

The effect of stage-cut on both CO_2 purity and recovery was studied by varying the membrane area in m^2 in the simulated process. As seen in Fig. 10, increasing stage-cut increases the recovery of the membrane while significantly affecting the purity of the processed stream. In this study, since the field testing which corresponded to the lowest stage-cut, the conditions of field test yielded the highest obtainable purity. The achievable CO_2 purity in the treated stream after a single-stage purification is in the range of membranes reported earlier [12,45,46]. Such high purity in a single-stage is beneficial to achieve an economically favourable CO_2 capture and purity. Nevertheless, the economic benefit of the fabricated membranes, especially with the ones containing mobile carriers, is clearly established in terms of the membrane area requirement for the same target recovery in Fig. 10B. It can be seen that the use of mobile carriers significantly reduced the membrane area requirement and hence can correlate to major savings in terms of membrane capital costs [47]. For instance, to achieve a CO_2 recovery target of 90%, the HFTMs containing mobile carriers required ~33% lower membrane area when compared to HFTMs. Similar benefits are obtained with purity CO_2 targets (Fig. 10B).

In order to benchmark the developed membranes with potential membranes for CO_2 separation, the performance of the current membranes as a single-stage separation unit has been compared with other hollow fiber CO_2 separation membranes with validation in pre-pilot scale or higher as seen in Table 5.

4. Conclusions

Hollow fiber modules with hybrid facilitated transport membranes were fabricated in the pre-pilot scale and tested in field conditions using real flue gas at a cement plant. Operation conditions such as feed pressure, temperature and pressure ratio were optimized to maximize separation using hybrid facilitated transport membrane. The HFTMs containing mobile carriers clearly showed improved performances than the neat HTFMs, indicating the advantages of CO_2-philic additives in membranes for post-combustion capture. Higher water content in the feed stream led to better performances, but temperature fluctuations close to saturation might risk water condensation in the modules. Elevated temperature and reliable water profile in the real flue gas enhanced the permeation properties of the membrane modules when compared to the labscale tests. Long-term testing of HFTM in untreated flue gas revealed the good performance durability of the membrane for a period of two weeks. The HFTMs with mobile carriers were subjected to resistance testing for SO_2 and NO impurities in simulated flue gas, and no obvious changes in CO_2 permeate purity were obtained. Simulation studies reveal that, to achieve the first stage separation of a typical post-combustion capture process, use of the fabricated membranes leads to significant improvements in the separation performance compared to the currently available hollow fiber membranes tested at pre-pilot scale or higher, thus leading to decreased membrane area requirements. However, to further study the cost benefits of the HFTMs in a large scale process, extended exposure tests should be performed in order to estimate the membrane life time. Nevertheless, the developed high-performance membranes tested in the relevant environment strengthens the commercial potential of implementing membrane technology in CO_2 separation applications.

Author contributions

S.J. L.A. and L.D. designed the experiments. S.J. and A.L. fabricated the membranes, S.J., F.S., R.C., and G.M.N. performed the permeation tests in the field. K.M. carried out tests at PACT and analyzed the corresponding results. S.J. analysed all the other results and wrote the manuscript. L.D. conceived the original idea, planned the overall study and supervised the research work.

Declaration of Competing Interest

The authors declare that they have no known competing financial interests or personal relationships that could have appeared to influence the work reported in this paper.

Acknowledgements

This work is a part of the NANOMEMC2 project supported by the European Union's Horizon 2020 Research and Innovation program under Grant Agreement n° 727734 and the FaT H2 project supported by the Research Council of Norway (No. 294533). The authors thank Prof. Marco Giacinti Baschetti for the collaboration and logistic support from University of Bologna. The authors also thank Janos Szuhanski, Muhammad Akram, Mohammad S Ismail, Karen N Finney and Prof. Mohamed Pourkashanian from USFD. The Research Council of Norway is acknowledged for the support to the Norwegian Micro- and Nano-Fabrication Facility, NorFab, project number 245963/F50.

Appendix A. Supplementary data

Supplementary data to this article can be found online at https://doi.org/10.1016/j.cej.2020.127405.

References

[1] National Oceanic and Atmospheric Administration, Carbon Dioxide, NASA. (2020). https://climate.nasa.gov/vital-signs/carbon-dioxide/.
[2] M. Bui, C.S. Adjiman, A. Bardow, E.J. Anthony, A. Boston, S. Brown, P.S. Fennell, S. Fuss, A. Galindo, L.A. Hackett, J.P. Hallett, H.J. Herzog, G. Jackson, J. Kemper, S. Krevor, G.C. Maitland, M. Matuszewski, I.S. Metcalfe, C. Petit, G. Puxty, J. Reimer, D.M. Reiner, E.S. Rubin, S.A. Scott, N. Shah, B. Smit, J.P.M. Trusler, P. Webley, J. Wilcox, N. Mac Dowell, Carbon capture and storage (CCS): the way forward, Energy Environ. Sci. 11 (2018) 1062–1176, https://doi.org/10.1039/c7ee02342a.
[3] B.P. Spigarelli, S.K. Kawatra, Opportunities and challenges in carbon dioxide capture, J. CO_2 Util. 1 (2013) 69–87, https://doi.org/10.1016/j.jcou.2013.03.002.
[4] Y. Han, W.S.W. Ho, Recent advances in polymeric membranes for CO_2 capture, Chinese J. Chem. Eng. 26 (2018) 2238–2254, https://doi.org/10.1016/j.cjche.2018.07.010.
[5] S. Janakiram, M. Ahmadi, Z. Dai, L. Ansaloni, L. Deng, Performance of nanocomposite membranes containing 0D to 2D nanofillers for CO_2 separation: a review, Membranes (Basel). 8 (2018), https://doi.org/10.3390/membranes8020024.
[6] H.B. Park, J. Kamcev, L.M. Robeson, M. Elimelech, B.D. Freeman, Maximizing the right stuff: The trade-off between membrane permeability and selectivity, Science (80) 356 (2017) eaab0530, https://doi.org/10.1126/science.aab0530.
[7] S. Li, Z. Wang, C. Zhang, M. Wang, F. Yuan, J. Wang, S. Wang, Interfacially polymerized thin film composite membranes containing ethylene oxide groups for CO_2 separation, J. Memb. Sci. 436 (2013) 121–131, https://doi.org/10.1016/j.memsci.2013.02.038.
[8] D. Leeson, N. Mac Dowell, N. Shah, C. Petit, P.S. Fennell, A Techno-economic analysis and systematic review of carbon capture and storage (CCS) applied to the iron and steel, cement, oil refining and pulp and paper industries, as well as other high purity sources, Int. J. Greenh. Gas Control. 61 (2017) 71–84, https://doi.org/10.1016/j.ijggc.2017.03.020.
[9] Z. Dai, S. Fabio, N. Giuseppe Marino, C. Riccardo, L. Deng, Field test of a pre-pilot scale hollow fiber facilitated transport membrane for CO_2 capture, Int. J. Greenh. Gas Control. 86 (2019) 191–200, https://doi.org/10.1016/j.ijggc.2019.04.027.
[10] L. Zhao, E. Riensche, L. Blum, D. Stolten, Multi-stage gas separation membrane processes used in post-combustion capture: energetic and economic analyses, J. Memb. Sci. 359 (2010) 160–172, https://doi.org/10.1016/j.memsci.2010.02.003.
[11] B. Wetenhall, J.M. Race, M.J. Downie, The effect of CO_2 purity on the development of pipeline networks for carbon capture and storage schemes, Int. J. Greenh. Gas Control. 30 (2014) 197–211, https://doi.org/10.1016/j.ijggc.2014.09.016.
[12] D. Yang, Z. Wang, J. Wang, S. Wang, Potential of two-stage membrane system with recycle stream for CO_2 capture from postcombustion gas, Energy Fuels 23 (2009) 4755–4762, https://doi.org/10.1021/ef801109p.
[13] P. Klingberg, K. Wilkner, M. Schlüter, J. Grünauer, S. Shishatskiy, Separation of carbon dioxide from real power plant flue gases by gas permeation using a supported ionic liquid membrane: an investigation of membrane stability, Membranes (Basel). 9 (2019), https://doi.org/10.3390/membranes9030035.
[14] A.M. Arias, M.C. Mussati, P.L. Mores, N.J. Scenna, J.A. Caballero, S.F. Mussati, Optimization of multi-stage membrane systems for CO_2 capture from flue gas, Int. J. Greenh. Gas Control. 53 (2016) 371–390, https://doi.org/10.1016/j.ijggc.2016.08.005.
[15] S. Janakiram, J.L. Martín Espejo, K.K. Høisæter, A. Lindbråthen, L. Ansaloni, L. Deng, Three-phase hybrid facilitated transport hollow fiber membranes for enhanced CO_2 separation, Appl. Mater. Today. 21 (2020), 100801, https://doi.org/10.1016/j.apmt.2020.100801.
[16] S. Janakiram, J. Luis Martín Espejo, X. Yu, L. Ansaloni, L. Deng, Facilitated transport membranes containing graphene oxide-based nanoplatelets for CO_2 separation: Effect of 2D filler properties, J. Memb. Sci. 616 (2020), 118626, https://doi.org/10.1016/j.memsci.2020.118626.
[17] N.C. Mat, G.G. Lipscomb, Membrane process optimization for carbon capture, Int. J. Greenh. Gas Control. 62 (2017) 1–12, https://doi.org/10.1016/j.ijggc.2017.04.002.
[18] T.C. Merkel, H. Lin, X. Wei, R. Baker, Power plant post-combustion carbon dioxide capture: an opportunity for membranes, J. Memb. Sci. 359 (2010) 126–139, https://doi.org/10.1016/j.memsci.2009.10.041.
[19] J. Franz, S. Schiebahn, L. Zhao, E. Riensche, V. Scherer, D. Stolten, Investigating the influence of sweep gas on CO_2/N_2 membranes for post-combustion capture, Int. J. Greenh. Gas Control. 13 (2013) 180–190, https://doi.org/10.1016/j.ijggc.2012.12.008.
[20] Y. Zhao, B.T. Jung, L. Ansaloni, W.S.W. Ho, Multiwalled carbon nanotube mixed matrix membranes containing amines for high pressure CO_2/H_2 separation, J. Memb. Sci. 459 (2014) 233–243, https://doi.org/10.1016/j.memsci.2014.02.022.
[21] R.W. Baker, Membrane Technology and Applications, 2004. doi: 10.1016/S0376-7388(00)83139-7.
[22] H. Liu, Y. Shao, Predictions of the impurities in the CO_2 stream of an oxy-coal combustion plant, Appl. Energy. 87 (2010) 3162–3170, https://doi.org/10.1016/j.apenergy.2010.04.014.
[23] C.A. Hall, K.A. Le, C. Rudaz, A. Radhi, C.S. Lovell, R.A. Damion, T. Budtova, M. E. Ries, Macroscopic and microscopic study of 1-Ethyl-3-methyl-imidazolium acetate-water mixtures, J. Phys. Chem. B. 116 (2012) 12810–12818, https://doi.org/10.1021/jp306829c.
[24] J.A. Lim, D.H. Kim, Y. Yoon, S.K. Jeong, K.T. Park, S.C. Nam, Absorption of CO_2 into aqueous potassium salt solutions of l -alanine and l -proline, Energy Fuels 26 (2012) 3910–3918, https://doi.org/10.1021/ef300453e.
[25] L. Deng, T.J. Kim, M.B. Hägg, Facilitated transport of CO_2 in novel PVAm/PVA blend membrane, J. Memb. Sci. 340 (2009) 154–163, https://doi.org/10.1016/j.memsci.2009.05.019.
[26] D. Venturi, D. Grupkovic, M.G. Baschetti, L. Sisti, Effect of humidity and nanocellulose content on Polyvinylamine-nanocellulose hybrid membranes for CO_2 capture, J. Memb. Sci. (2017), https://doi.org/10.1016/j.memsci.2017.11.021.
[27] X. He, C. Fu, M.B. Hägg, Membrane system design and process feasibility analysis for CO_2 capture from flue gas with a fixed-site-carrier membrane, Chem. Eng. J. 268 (2015) 1–9, https://doi.org/10.1016/j.cej.2014.12.105.
[28] E. Santos, J. Albo, A. Irabien, Acetate based supported ionic liquid membranes (SILMs) for CO_2 separation: influence of the temperature, J. Memb. Sci. 452 (2014) 277–283, https://doi.org/10.1016/j.memsci.2013.10.024.
[29] S. Shen, Y. Nan Yang, Y. Wang, S. Ren, J. Han, A. Chen, CO_2 absorption into aqueous potassium salts of lysine and proline: density, viscosity and solubility of CO_2, Fluid Phase Equilib. 399 (2015) 40–49, https://doi.org/10.1016/j.fluid.2015.04.021.
[30] M. Sandru, T.J. Kim, W. Capala, M. Huijbers, M.B. Hägg, Pilot scale testing of polymeric membranes for CO_2 capture from coal fired power plants, Energy Procedia 37 (2013) 6473–6480, https://doi.org/10.1016/j.egypro.2013.06.577.
[31] M.B. Hägg, A. Lindbråthen, X. He, S.G. Nodeland, T. Cantero, Pilot demonstration-reporting on CO_2 capture from a cement plant using hollow fiber process, Energy Procedia 114 (2017) 6150–6165, https://doi.org/10.1016/j.egypro.2017.03.1752.
[32] X. He, A. Lindbråthen, T.J. Kim, M.B. Hägg, Pilot testing on fixed-site-carrier membranes for CO_2 capture from flue gas, Int. J. Greenh. Gas Control. 64 (2017) 323–332, https://doi.org/10.1016/j.ijggc.2017.08.007.
[33] Y. Zhao, W.S.W. Ho, Steric hindrance effect on amine demonstrated in solid polymer membranes for CO_2 transport, J. Memb. Sci. 415–416 (2012) 132–138, https://doi.org/10.1016/j.memsci.2012.04.044.
[34] J. Pohlmann, M. Bram, K. Wilkner, T. Brinkmann, Pilot scale separation of CO_2 from power plant flue gases by membrane technology, Int. J. Greenh. Gas Control. 53 (2016) 56–64, https://doi.org/10.1016/j.ijggc.2016.07.033.
[35] Y. Han, W. Salim, K.K. Chen, D. Wu, W.S.W. Ho, Field trial of spiral-wound facilitated transport membrane module for CO_2 capture from flue gas, J. Memb. Sci. 575 (2019) 242–251, https://doi.org/10.1016/j.memsci.2019.01.024.
[36] C.A. Scholes, S.E. Kentish, G.W. Stevens, Effects of minor components in carbon dioxide capture using polymeric gas separation membranes, Sep. Purif. Rev. 38 (2009) 1–44, https://doi.org/10.1080/15422110802411442.
[37] G.S. Goff, G.T. Rochelle, Monoethanolamine degradation: O_2 mass transfer effects under CO_2 capture conditions, Ind. Eng. Chem. Res. 43 (2004) 6400–6408, https://doi.org/10.1021/ie0400245.
[38] K. Knoblauch, E. Richter, H. Jüntgen, Application of active coke in processes of SO_2- and NO_x-removal from flue gases, Fuel 60 (1981) 832–838, https://doi.org/10.1016/0016-2361(81)90146-0.
[39] L.S. White, X. Wei, S. Pande, T. Wu, T.C. Merkel, Extended flue gas trials with a membrane-based pilot plant at a one-ton-per-day carbon capture rate, J. Memb. Sci. 496 (2015) 48–57, https://doi.org/10.1016/j.memsci.2015.08.003.
[40] K. Okabe, N. Matsumiya, H. Mano, Stability of gel-supported facilitated transport membrane for carbon dioxide separation from model flue gas, Sep. Purif. Technol. 57 (2007) 242–249, https://doi.org/10.1016/j.seppur.2007.04.007.
[41] S. Li, Z. Wang, W. He, C. Zhang, H. Wu, J. Wang, S. Wang, Effects of minor SO2 on the transport properties of fixed carrier membranes for CO_2 capture, Ind. Eng. Chem. Res. 53 (2014) 7758–7767, https://doi.org/10.1021/ie404063r.
[42] T.J. Kim, H. Vrålstad, M. Sandru, M.B. Hägg, Separation performance of PVAm composite membrane for CO_2 capture at various pH levels, J. Memb. Sci. 428 (2013) 218–224, https://doi.org/10.1016/j.memsci.2012.10.009.
[43] T.J. Kim, M.W. Uddin, M. Sandru, M.B. Hägg, The effect of contaminants on the composite membranes for CO_2 separation and challenges in up-scaling of the membranes, Energy Procedia 4 (2011) 737–744, https://doi.org/10.1016/j.egypro.2011.01.113.
[44] D. Wu, C. Sun, P.K. Dutta, W.S. Winston Ho, SO_2 interference on separation performance of amine-containing facilitated transport membranes for CO_2 capture from flue gas, J. Memb. Sci. 534 (2017) 33–45, https://doi.org/10.1016/j.memsci.2017.04.003.
[45] A. Hussain, M.B. Hägg, A feasibility study of CO_2 capture from flue gas by a facilitated transport membrane, J. Memb. Sci. 359 (2010) 140–148, https://doi.org/10.1016/j.memsci.2009.11.035.
[46] K.T. Woo, G. Dong, J. Lee, J.S. Kim, Y.S. Do, W.H. Lee, H.S. Lee, Y.M. Lee, Ternary mixed-gas separation for flue gas CO_2 capture using high performance thermally rearranged (TR) hollow fiber membranes, J. Memb. Sci. 510 (2016) 472–480, https://doi.org/10.1016/j.memsci.2016.03.033.
[47] M.T. Ho, G.W. Allinson, D.E. Wiley, Reducing the cost of CO_2 capture from flue gases using membrane technology, Ind. Eng. Chem. Res. 47 (2008) 1562–1568, https://doi.org/10.1021/ie070541y.
[48] S.H. Choi, J.H. Kim, Y. Lee, Pilot-scale multistage membrane process for the separation of CO_2 from LNG-fired flue gas, Sep. Purif. Technol. 110 (2013) 170–180, https://doi.org/10.1016/j.seppur.2013.03.016.
[49] C.A. Scholes, A. Qader, G.W. Stevens, S.E. Kentish, Membrane gas-solvent contactor pilot plant trials of CO_2 absorption from flue gas, Greenh. Gases Sci. Technol. 5 (2014) 229–237, https://doi.org/10.1080/01496395.2014.937499.